Optimizing Ligand Charges for Maximum Binding Affinity. A Solvated Interaction Energy Approach

Traian Sulea and Enrico O. Purisima*

Biotechnology Research Institute, National Research Council of Canada, 6100 Royalmount Avenue, Montreal, Quebec H4P 2R2, Canada

Received: October 20, 2000

We show that for a given binding site and a given spatial arrangement of atoms in a ligand, there exists an optimal set of partial charges at the atom centers that will optimize the net electrostatic binding free energy of the ligand. This optimal value can be calculated quite readily from a simple quadratic polynomial with coefficients derivable from a few continuum dielectric solvation calculations using a boundary element (BEM) solution of the Poisson equation. Three examples are presented: (a) the binding of cations to 18-crown-6 ether, (b) the calcium-binding sites of parvalbumin, and (c) ligand binding at the active site of the cysteine protease, cathepsin B. The calculations indicate that potassium is the preferred cation for binding to 18-crown-6 ether and that its charge of 1 eu is close to optimal for binding affinity. Similarly, the optimum charge for a monatomic ligand (with a calcium radius) in the calcium binding sites of parvalbumin is predicted to be about 1.8 eu, in agreement with this site's preference for divalent cations. These results show how electrostatics provides a mechanism for binding site specificity for a given ionic valency. For cathepsin B, charge preferences around the active site are probed using both monatomic and multiatomic ligands. The notion of charge complementarity should be extended beyond the pairing of oppositely charged groups to also include the selection of the correct charge magnitudes. The concept of optimum ligand charges has profound implications for understanding molecular recognition and for molecular design.

Introduction

In recent years, the depiction of molecular surfaces that are color-coded by electrostatic potential has been a popular and useful method for visualizing the electrostatic profile of binding sites. Such images produced by the program GRASP[1], for example, provide a global understanding of the electrostatic characteristics of a molecule and quickly focus attention on regions with propensities to bind charged or polar groups. Such maps highlight the property of electrostatic complementarity as a necessary ingredient for good binding interactions. For example, it is intuitively clear that a binding site with a negative electrostatic potential would selectively recognize positively charged atoms or groups. However, this picture of complementarity is not as simple as it seems. Consider the negative-potential binding site just mentioned above. If it binds a monatomic ion with a +1 charge, would it necessarily bind an ion with a +2, +3, or +4 charge with better affinity, assuming no steric problems? Let us suppose that the series of ions have identical radii and van der Waals interactions with the binding site. On the basis of electrostatic complementarity, it would seem that a positively charged ion would bind with monotonically increasing strength as its charge becomes more positive. In fact, this is not the case. For this monatomic ion, there exists a finite optimum charge that optimizes the binding energy. As pointed out by Lee and Tidor, the reason is that although increasing the charge of the ion will strengthen its interactions with the binding site, it will also strengthen its interactions with the solvent in the unbound state.[2] Which one wins out depends on the magnitude of the charge, the shape of the solute cavity, and the charge distribution in it. In general, for a given binding site and a given spatial arrangement of atoms in a ligand, there exists a unique optimal set of partial charges on the atom centers that will optimize the net electrostatic binding free energy of the ligand. What this means is that electrostatics provides a mechanism for molecular recognition based not only on polarity but also on the magnitude of the charge as well. Tidor and coworkers have recently described a method for calculating an optimal multipole charge distribution for spherical ligands.[2−6] However, extension of the results to a realistic molecular description was not straightforward.

In this paper, we show how the optimal atom-centered charges can be calculated quite readily from a simple quadratic polynomial with coefficients derivable from a few continuum dielectric solvation calculations using a boundary element (BEM) solution of the Poisson equation. The use of this polynomial avoids the computationally expensive repeated solution of the Poisson equation in mapping out the charge dependence of the binding free energy. We describe applications to three examples: (a) an 18-crown-6 ether that binds monatomic ions, (b) calcium binding sites in parvalbumin, and (c) the active site of cathepsin B, a cysteine protease with carboxypeptidase activity due to a favorable binding site for a carboxylate group.

Theory

In the continuum dielectric model, the total electrostatic free energy of assembling solute charges from infinite separation into a cavity with dielectric constant, D_{in}, surrounded by an external continuum medium with dielectric constant, D_{out}, is given by

$$G = \frac{1}{2}\sum_i q_i\phi = \frac{1}{2}\sum_i q_i(\phi^C + \phi^R) \qquad (1)$$

* Corresponding author. E-mail: enrico.purisima@bri.nrc.ca.

10.1021/jp0038714 CCC: $20.00 Published 2001 by the American Chemical Society
Published on Web 01/03/2001

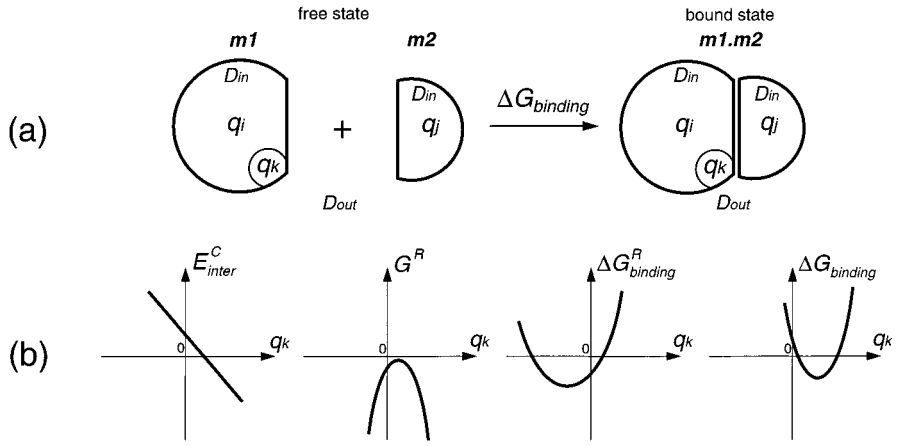

Figure 1. (a) Schematic diagram of the binding of two molecules. We wish to find the optimal values for one or more charges q_k in the ligand m_1 that maximizes binding affinity to m_2. A continuum dielectric approximation is used with D_{in} and D_{out} representing the solute and solvent dielectric constants. (b) Qualitative dependence of various components of the electrostatic binding free energy on the charge q_k. The intermolecular Coulomb interaction energy is a linear function of the charge. The reaction field energy of the free and bound states are parabolic functions of the charge, with the curvature in the free state steeper than that in the bound state. The difference between the reaction field energies of the bound and free states is another parabola that opens upward instead of downward, resulting in a finite minimum value. The addition of the linear Coulomb term merely shifts this parabola to the final one representing the total electrostatic binding free energy. In the text of this paper, we describe how to rapidly calculate the coefficients of the quadratic form representing the dependence of the binding free energy on the ligand charges. The optimal ligand charges can then be derived immediately.

where the summation is over the solute charges and ϕ is the potential at the position of charge q_i. ϕ^C and ϕ^R are the Coulomb and reaction field potentials, respectively. The reaction field potential is due to the induced surface charge distribution at the dielectric boundary. These potentials are computed as

$$\phi_i^{\mathrm{C}} = \frac{1}{D_{\mathrm{in}}} \sum_{j \neq i} \frac{q_j}{r_{ij}} \tag{2}$$

$$\phi_i^{\mathrm{R}} = \int_S \frac{\sigma(\mathbf{r})}{|\mathbf{r} - \mathbf{r}_i|} \, \mathrm{d}S \tag{3}$$

where $\sigma(\mathbf{r})$ is the induced surface charge density and the integral is taken over the entire surface enclosing the cavity. The determination of the induced surface charge distribution and the reaction field potential can be carried out using boundary element methods.[7−11]

When two solute molecules, m_1 and m_2, associate to form a molecular complex in solution (Figure 1a), the electrostatic free energy of binding is given by the difference between the free energies in the bound and free states

$$\Delta G_{\mathrm{binding}} = G_{\mathrm{bound}} - G_{\mathrm{free}} \tag{4}$$

(From this point on, the terms free energy and energy will implicitly mean the electrostatic components of these quantities unless explicitly qualified.) Using eq 1, we can rewrite the binding free energy as

$$\Delta G_{\mathrm{binding}} = E_{\mathrm{inter}}^{\mathrm{C}} + \Delta G_{\mathrm{binding}}^{\mathrm{R}} \tag{5}$$

where $E_{\mathrm{inter}}^{\mathrm{C}}$ is the intermolecular Coulomb interaction energy between molecules m_1 and m_2 in the bound state and $\Delta G_{\mathrm{binding}}^{\mathrm{R}}$ is the change in reaction field energy upon binding. To derive the functional dependence of the electrostatic binding free energy on the solute charges, let us consider a particular charge q_k in molecule m_1 (Figure 1a) and determine the dependence of each of terms in eq 5 on q_k. The Coulomb interaction energy is

$$E_{\mathrm{inter}}^{\mathrm{C}} = \sum_{i \in m_1} q_i \phi_{m_2}^{\mathrm{C}} = \frac{1}{D_{\mathrm{in}}} \sum_{i \in m_1} q_i \sum_{j \in m_2} q_j / r_{ij} \tag{6}$$

The linear dependence on q_k of the Coulomb term can be readily obtained by rewriting eq 6 as

$$E_{\mathrm{inter}}^{\mathrm{C}} = \frac{1}{D_{\mathrm{in}}} \left(q_k \sum_{j \in m_2} q_j / r_{kj} + \sum_{i \in m_1 - k} q_i \sum_{j \in m_2} q_j / r_{ij} \right) = c_1 q_k + c_0 \tag{7}$$

where $m_1 - k$ means molecule m_1 excluding charge q_k. The reaction field component is given by

$$\Delta G_{\mathrm{binding}}^{\mathrm{R}} = \frac{1}{2} \left(\sum_{i \in m_1 . m_2} q_i \phi_{m_1 . m_2}^{\mathrm{R}} \right)_{\mathrm{bound}} - \frac{1}{2} \left(\sum_{i \in m_1} q_i \phi_{m_1}^{\mathrm{R}} + \sum_{j \in m_2} q_j \phi_{m_2}^{\mathrm{R}} \right)_{\mathrm{free}} \tag{8}$$

where $\phi_{m_1 . m_2}^{\mathrm{R}}$, $\phi_{m_1}^{\mathrm{R}}$, and $\phi_{m_2}^{\mathrm{R}}$ are the reaction field potentials of the complex $m_1.m_2$ and the two individual molecules in the free state, respectively. Assuming a linear response of the dielectric, the total reaction field is the superposition of all the individual reaction fields of the charges in the cavity

$$\phi^{\mathrm{R}} = \sum_i \phi_i^{\mathrm{R}} \tag{9}$$

where ϕ_i^{R} is the reaction field potential due to charge q_i with all the other charges in the cavity set to zero. Using eq 9, we can rewrite the expression for the free state in eq 8 as

$$G_{\mathrm{free}}^{\mathrm{R}} = \frac{1}{2} \left[q_k (\phi_k^{\mathrm{R}} + \phi_{m_1 - k}^{\mathrm{R}}) + \sum_{i \in m_1 - k} q_i (\phi_k^{\mathrm{R}} + \phi_{m_1 - k}^{\mathrm{R}}) + \sum_{j \in m_2} q_j \phi_{m_2}^{\mathrm{R}} \right] \tag{10}$$

where $\phi_{m_1 - k}^{\mathrm{R}}$ is the reaction field potential due to the charges of

m_1 with the charge q_k set to zero. A property of the reaction field potential produced by the charge, q_k, is that it is proportional to q_k and opposite in sign[12]

$$\phi_k^{\mathrm{R}} \sim -q_k \tag{11}$$

This allows us to regroup the terms in eq 10 into quantities that are quadratic, linear, and constant with respect to the charge, q_k

$$G_{free}^{R} = \frac{1}{2}\Big(\underbrace{q_k\phi_k^R}_{\text{quadratic}} + \underbrace{q_k\phi_{m_1-k}^R + \sum_{i\in m_1-k} q_i\phi_k^R}_{\text{linear}} + \underbrace{\sum_{i\in m_1-k} q_i\phi_{m_1-k}^R + \sum_{j\in m_2} q_j\phi_{m_2}^R}_{\text{constant}} \Big) \tag{12}$$

The dependence on q_k in eq 12 can be written more explicitly by noting that eq 11 implies that

$$\phi_k^{\mathrm{R}} = q_k\phi_{q_k=1}^{\mathrm{R}} \tag{13}$$

where $\phi_{q_k=1}^{\mathrm{R}}$ is the reaction field potential of a unit charge located at the position of q_k. Note that $\phi_{q_k=1}^{\mathrm{R}}$ in the right-hand side of eq 13 has units of potential/unit charge. Equations 12 and 13 then give

$$G_{free}^{R} = \frac{1}{2}\Big(\underbrace{q_k^2\phi_{q_k=1}^R}_{\text{quadratic}} + \underbrace{q_k\phi_{m_1-k}^R + q_k\sum_{i\in m_1-k} q_i\phi_{q_k=1}^R}_{\text{linear}} + \underbrace{\sum_{i\in m_1-k} q_i\phi_{m_1-k}^R + \sum_{j\in m_2} q_j\phi_{m_2}^R}_{\text{constant}} \Big) \tag{14}$$

We see that reaction field energy has a quadratic functional form

$$G_{\mathrm{free}}^{\mathrm{R}} = c_2q_k^2 + c_1q_k + c_0 \tag{15}$$

and that the reaction field energy can be rapidly calculated for an arbitrary value of q_k once we have the c_x coefficients. Equation 14 shows that these coefficients can be obtained readily with just three calculations: one for the potential due to a unit charge at the position of q_k with all other m_1 charges zeroed, one for the potential due to all other m_1 charges with q_k zeroed, and one for the potential due to m_2 in the free state

$$c_2 = \frac{1}{2}\phi_{q_k=1}^{\mathrm{R}}(\vec{r}_k)$$

$$c_1 = \frac{1}{2}[\phi_{m_1-k}^{\mathrm{R}}(\vec{r}_k) + \sum_{i\in m_1-k} q_i\phi_{q_k=1}^{\mathrm{R}}(\vec{r}_i)] \tag{16}$$

$$c_0 = \frac{1}{2}[\sum_{i\in m_1-k} q_i\phi_{m_1-k}^{\mathrm{R}}(\vec{r}_i) + \sum_{j\in m_2} q_j\phi_{m_2}^{\mathrm{R}}(\vec{r}_j)]$$

In eq 16, we have explicitly indicated the position at which the reaction field potential is to be evaluated; e.g., $\vec{r}_i$ refers to the coordinates of charge i.

Since the reaction field potential of a unit charge is negative, we have the important relation that $c_2 < 0$. This means that the reaction field energy is unbounded from below, i.e.

$$G_{\mathrm{free}}^{\mathrm{R}} \rightarrow -\infty \qquad \text{as} \qquad |q_k| \rightarrow \infty \tag{17}$$

The derivation of the dependence on q_k of the reaction field energy for the complex results in a similar quadratic functional form also with its $c_2 < 0$. Thus, the change in reaction field energy upon binding has a quadratic functional form

$$\Delta G_{\mathrm{binding}}^{\mathrm{R}} = G_{\mathrm{bound}}^{\mathrm{R}} - G_{\mathrm{free}}^{\mathrm{R}} = c_2q_k^2 + c_1q_k + c_0 \tag{18}$$

where $c_x = c_x(\mathrm{bound}) - c_x(\mathrm{free})$. In general, the size of the cavity of the complex, $m_1.m_2$, is larger than the cavity formed by m_1 alone. This means that the $\phi_{q_k=1}^{\mathrm{R}}$ felt by q_k is smaller in magnitude (due to greater desolvation of q_k) in the complex than in the free state. This implies that $|c_2(\mathrm{free})| > |c_2(\mathrm{bound})|$ and hence $c_2 > 0$ in eq 18. Thus, the reaction field energy of binding has a well-defined unique minimum with respect to q_k. Addition of the Coulomb term, eq 7, which is linear, only shifts the location of the minimum and the value of the minimum energy. The qualitative dependence of the Coulomb energy, the reaction field energies, and the total electrostatic free energy of binding is shown schematically in Figure 1b.

The above derivation can be generalized (see Appendix) to obtain the dependence of the binding free energy on n multiple charges. In that case, the free energy is a paraboloid in $n+1$-dimensional space with respect to the charges. Again, a unique minimum exists. The existence of a unique minimum in our formulation of the problem is in contrast with the nonuniqueness of the multipole charge distribution obtained when the positions of the charge centers in the molecular cavity are not fixed.[4]

Methods

18-Crown-6 Ether. The coordinates of the 18-crown-6 ether in complex with a potassium ion were taken from the crystal structure[13] (CSD code KCROFE) deposited in the Cambridge Structural Database. The partial charges used in the calculation were taken from Howard et al.[14] The dependence of the binding free energy on the ionic charge was then calculated for a series of ligand radii corresponding to alkali metal ions.

Calcium-Binding Site. The 1.5 Å-resolution crystal structure (PDB code 4cpv) of the carp parvalbumin complexed with two calcium ions[15] was retrieved from the Protein Data Bank. The water atoms were removed, and the hydrogen atoms were added explicitly. The protein atoms were assigned AMBER 4.1 partial charges.[16] The charge dependence of the binding free energy of a monatomic ion with a calcium radius was calculated for each of the calcium-binding sites.

Cathepsin B Active Site. The 2.0 Å-resolution crystal structure (PDB code 1csb) of the human cathepsin B complexed with the CA030 inhibitor[17] was retrieved from the Protein Data Bank. Ligand and water atoms were removed, hydrogen atoms were added, and partial charges assigned as in the parvalbumin example. In the case of cathepsin B, the catalytic cysteine and histidine residues were considered in the ion-pair state, and the histidine residues were protonated, consistent with the pH dependence of cathepsin B-catalyzed hydrolyses.[18,19] The charge dependence of the binding free energy at selected positions around the active site was examined using monatomic probes and an acetate molecule.

Binding Free Energy Calculation. The intermolecular Coulomb interaction energy term was calculated using a dielectric constant of 2 and infinite cutoff. The electrostatic contribution to solvation was calculated using a continuum

TABLE 1: Born Radii Used for Reaction Field Calculations Involving Metal Ions and the Calculated and Observed Free Energies of Hydration for These Ions[a]

ion	R_{Born} (Å)	$\Delta G^{calc}_{hydration}$	$\Delta G^{obs\ b}_{hydration}$	$\Delta G^{obs\ c}_{hydration}$
Li^+	1.3161	−124.6	−122.1	−115.0
Na^+	1.7013	−96.4	−98.2	−89.7
K^+	2.0865	−78.6	−80.6	−72.7
Rb^+	2.2363	−73.3	−75.5	−67.2
Cs^+	2.4610	−66.6	−67.8	−61.7
Ca^{2+}	1.7120	−383.1	−380.8	−362.0

[a] The free energies are in kcal/mol. The Born radii, R_{Born}, are derived from the calculated ion−water radial distribution function (RDF) peaks[24] using the formula[25,26] $R_{Born} = 1.07(R_{I-w} - 0.8)$, where R_{I-w} is the ion−water RDF peak. The calculated hydration free energies are derived directly from the Born formula, $0.5q^2(1 - 1/\epsilon_{solv})/R_{Born}$. [b] Experimental values from Burgess,[27] as tabulated in Åqvist.[24] [c] Experimental values from Marcus.[28]

TABLE 2: Coefficients for the Dependencies of Various Energy Terms on the Charge of the Potassium Ion in Binding to the 18-Crown-6 Ether

	$c_2(q_K^2)$	$c_1(q_K)$	c_0
E^C_{inter}	–	−31.1607	–
G^R_{bound}	−30.0746	13.3669	−4.6595
G^R_K	−38.7859	–	–
G^R_{host}	–	–	−6.8300
$\Delta G^R_{binding}$	8.7113	13.3669	2.1705
$\Delta G_{binding}$	8.7113	−17.7938	2.1705

dielectric model. A dielectric constant of 2 was used for the solute interior, and a dielectric constant of 78.5 was applied for the exterior medium (solvent water). The reaction field energies were computed using the BRI BEM program[20,21] and the SIMS molecular surface program.[22] The atomic radii used for reaction field energy calculations were taken from the AMBER 4.1 van der Waals radii[16] with two modifications: the radius of polar hydrogens was set to 1.0 Å, and the carboxylate O radius was reduced to 1.5 Å. These radii were found to reproduce the solvation free energies of a test set of small molecules quite well.[23] In the case of metal ions only, the Born radii used for reaction field energy calculations were derived from the ion−water oxygen radial distribution function peaks[24] which were corrected for the water oxygen "core" as suggested by Rashin et al.[25,26] Table 1 lists the radii used for the metal ions as well as the calculated and experimental solvation energies for these ions. There is close agreement between the calculated and experimental solvation energies of Burgess[27] and somewhat worse but still good agreement with the experimental values of Marcus.[28] This suggests that the radii used for the metal ions are reasonable. The dependence of the binding free energy on atomic charge was calculated as described in the Theory section.

Results

18-Crown-6 Ether. The host−guest complex of the 18-crown-6 ether with alkali metal ions is our first test case for illustrating the concept of an optimal charge and dissecting the energy components that lead to that optimal charge. Table 2 lists the coefficients for the charge dependence of each of the energy components for an ion with a K^+ Born radius. The quadratic dependence of the binding free energy on ion charge is shown in Figure 2a. The charge that minimizes the binding free energy is 1.02 eu, close to the actual charge of a K^+ ion. In fact, the binding free energy of a +1 charge is only 0.004 kcal/mol above the minimum energy value. A neutral or divalent ion with the same radius is significantly higher in energy.

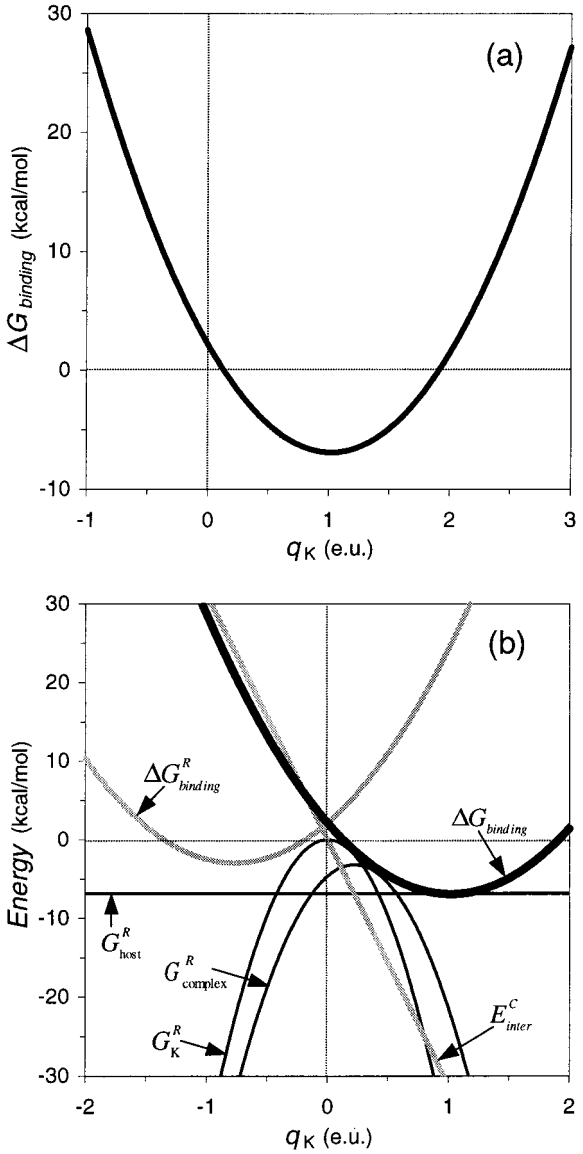

Figure 2. (a) Dependence of the binding free energy on the charge of a monatomic ligand (with a K^+ radius) bound to 18-crown-6 ether. (b) Charge dependence of the components of the total electrostatic binding free energy. Note that $G^R_{complex} - (G^R_K + G^R_{host})$ leads to a parabola for the reaction field energy of binding, $\Delta G^R_{binding}$, that opens upward and has finite minimum. Addition of the Coulomb term shifts the parabola to its final position.

Figure 2b shows the charge dependence of each of the components of the binding free energy. As expected from the exposition in the Theory section, the reaction field energy profiles of the bound and free states are parabolas that open downward. The difference of these two parabolas leads to a parabola, $\Delta G^R_{binding}$, that opens upward and has a finite minimum. The Coulomb interaction energy is a linear function of the charge which, when added to the $\Delta G^R_{binding}$ curve, shifts it to the final curve representing $\Delta G_{binding}$.

We also calculated the optimum charge for ions with radii corresponding to Li^+, Na^+, Rb^+, and Cs^+. A plot of the optimum charge versus radius is shown in Figure 3. We see that K^+ has a nearly ideal charge-radius combination. This is consistent with the experimental and theoretical finding that K^+ is the alkali cation that binds most strongly to 18-crown-6 ether in water.[29,30] Of course, van der Waals interactions also have to be taken into consideration to obtain a complete accounting of the binding

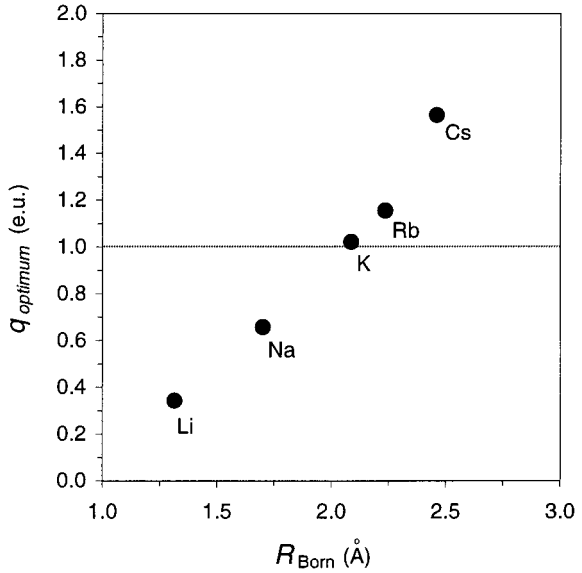

Figure 3. Optimum charge vs Born radius corresponding to a series of alkali metal ions bound to 18-crown-6 ether.

free energy. Nevertheless, these results show how electrostatics alone can contribute to selectivity.

Calcium-Binding Site. In a second test case for validating the charge optimization concept, we examined the complexation of the calcium ion with a calcium-binding protein, the carp parvalbumin. Two calcium ions bind to the parvalbumin molecule, one at the CD site and the other one at the EF site of the protein. We first examined the binding process of one ion (with its Born radius set to that of Ca^{2+}) to either calcium-binding site while the other site remained vacant. These systems are similar to the host−ion interaction example. We then subsequently analyzed the trimolecular process of binding two ions to the parvalbumin with simultaneous occupancy of both CD site and EF site.

Figure 4a shows the charge dependence of $\Delta G_{\text{binding}}$ for binding to either the CD or the EF site. The two sites show very similar charge dependencies of the binding free energy both in the location of the minimum and in the breadth of the curve. This suggests that the two calcium-binding sites are comparable in their tolerance to charge changes. The optimum charges obtained were 1.85 and 1.82 eu for the CD and EF sites, respectively. These optimal charges are also close to the actual charge of the Ca^{2+} cation, for which we obtain $\Delta G_{\text{binding}}$ values that are 0.714 and 0.947 kcal/mol above the minimum-energy values at the CD site and EF site, respectively. Reducing the charge to +1 or raising it to +3 increases the binding energy by about 20 or 40 kcal/mol, respectively, for either the CD or EF site. Table 3 lists the coefficients corresponding to the curves in Figure 4. We note that c_0 is close to zero for $\Delta G^{\text{R}}_{\text{binding}}$ for the CD site. This arises from the ligand being almost completely buried in the protein at the CD site. Since the molecular surface of the protein does not change between the free and bound states, the reaction field energy of the protein atoms remains the same for the two states.

Since the parvalbumin makes a 1:2 complex with calcium ions, we were interested in analyzing the binding of two calcium ions to the carp parvalbumin with simultaneous occupancy of both the CD site and the EF site. The comparison of the charge dependencies of $\Delta G_{\text{binding}}$ for the double- versus single-occupancy complexes would highlight the extent of mutual cooperativity between the two calcium-binding sites. Figure 5 shows the charge dependence of the binding free energy for

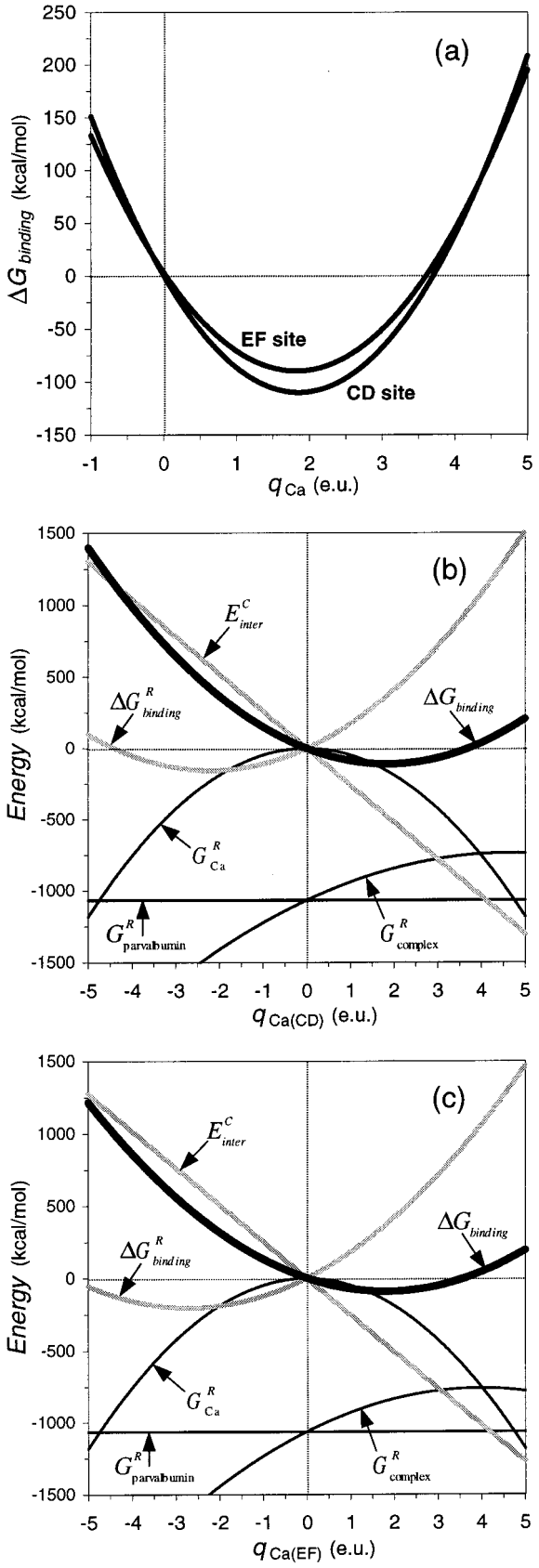

Figure 4. (a) Charge dependence of the binding free energy of a calcium ion in the CD and EF calcium-binding sites of parvalbumin. The curves are for the case of a singly occupied site. (b) Charge dependence of the components of the total electrostatic binding free energy for the CD site. (c) Charge dependence of the components of the total electrostatic binding free energy for the EF site.

TABLE 3: Coefficients for the Dependencies of Various Energy Terms on the Charge of the Calcium Ion that Binds to Either the CD or EF Site of Parvalbumin (single site occupancy)

	CD site			EF site		
	$c_2(q^2_{Ca(CD)})$	$c_1(q_{Ca(CD)})$	c_0	$c_2(q^2_{Ca(EF)})$	$c_1(q_{Ca(EF)})$	c_0
E^C_{inter}	–	−260.4742	–	–	−254.2912	–
G^R_{bound}	−15.1242	141.4714	−1065.5665	−19.1519	152.1367	−1062.5898
G^R_{Ca}	−47.2703	–	–	−47.2703	–	–
$G^R_{parvalbumin}$	–	–	−1065.5700	–	–	−1065.5700
$\Delta G^R_{binding}$	32.1461	141.4714	0.0035	28.1185	152.1367	2.9802
$\Delta G_{binding}$	32.1461	−119.0029	0.0035	28.1185	−102.1545	2.9802

this trimolecular association process. The minimum of the paraboloid occurs at an ionic charge of 1.82 and 1.79 eu for the CD and EF binding sites, respectively. These values are very close to the optimal charges for the single-occupancy complexes. The isoenergetic contours in Figure 5b shows that the principal axes of the paraboloid are almost parallel to the coordinate axes. This means that the binding free energy depends independently on each charge. This is seen more quantitatively in Table 4, where we see that the coefficient of the cross term involving the two charges is relatively small. Figure 5c shows cross sections passing through the minimum along each of the axes. We see that the breadth of the wells is very similar for the CD and EF sites, indicating similar charge selectivity. The similarity in shape of the curves and location of minima between the double- and single-occupancy case is consistent with the negligible cross-correlation between the two charges. All these observations suggest that there is little cooperativity between the two calcium binding sites of the studied protein (i.e., for the tested ligand, the optimal charge at one site is rather insensitive to the presence or absence of a ligand at the other site). This is to be expected since the two charges are far from each other and are in binding sites close to the surface. This means that their interactions with one another are effectively screened by the induced surface polarization charge density, making the cross-terms small.

Binding of Fragments of the CA030 Inhibitor to Cathepsin B. The complex of human cathepsin B with the covalent epoxysuccinyl inhibitor CA030 was selected as a third system for testing the optimal charge concept. Cathepsin B is a papain-like cysteine protease with dipeptidyl carboxypeptidase hydrolytic activity. This distinct functional characteristic of cathepsin B is attributed to the occluding loop, a unique structural feature which restricts the primed region of the binding site beyond the S2′ subsite and provides two histidine residues (His110 and His111) for anchoring the C-terminal carboxylate group of the substrate. The high selectivity of the CA030 inhibitor for cathepsin B stems from its resemblance to the substrate. This inhibitor contains a two-amino-acid sequence, Ile−Pro, linked to the reactive group in such a way that the first residue, isoleucyl, is positioned in the S1′ hydrophobic pocket and the second residue, prolyl, is accommodated in the S2′ pocket of the enzyme. The free carboxylate group of the C-terminal prolyl residue interacts with the two histidines from the occluding loop of the protein.

Using the same methods as in the previous two examples, we studied the charge dependence of binding a monatomic ligand at each of three positions in the active site of cathepsin B. These positions are shown schematically in Figure 6, where the interaction of the inhibitor with the S′ subsites is shown. Two of these positions correspond to the oxygen atoms of the essential C-terminal carboxylate group of the Pro residue (designated in what follows as O1 for the oxygen atom that interacts with both His110 and His111, and as O2 for the other oxygen atom that interacts with His111 only). The third location was the Cδ methyl group of the Ile residue (treated as a united carbon atom and named Meδ). The O1 and O2 atoms were assigned radii of 1.50 Å, while the Meδ atom had a radius of 2.0 Å.

Figure 7 shows the charge dependence of the binding free energy for each of the positions. O1 and O2 have optimal charge values of −0.54 and −0.38 eu, respectively. For the Meδ atom, the optimal charge is 0.08 eu. The breadth of the curve for O1 is narrower than that for O2, indicating that this position is more selective for its optimal charge that the other positions. The coefficients corresponding to these curves are listed in Table 5.

These results correctly identify the preference of cathepsin B for negative partial charges at the positions occupied by the oxygen atoms of the carboxylate group of the CA030 inhibitor when bound to the enzyme. In contrast, a nearly neutral atom was found to be optimal for binding at the location corresponding to the Cδ methyl group of the Ile residue of the inhibitor. This is consistent with the structural features of the enzyme binding subsites in which O1 and O2 interact with the positively charged histidine residues His110 and His111, whereas Meδ binds to the hydrophobic S1′ pocket of the enzyme.

Perhaps the most interesting results of this study were those obtained from the analysis of acetate binding in the S2′ pocket of human cathepsin B. The acetate molecule consisted of four atoms—the carboxylate O1, O2, and C and a united atom methyl group, Me. These atoms were positioned according to the locations of analogous atoms in the C-terminal proline of CA030. The optimal charge distribution for binding was then determined. No constraint on the total charge was imposed. Table 6 lists the coefficients for the quadratic form describing this system. We note that, unlike the parvalbumin case, the coefficients of the charge cross terms are not negligible. This means that the dependence of the binding free energy on the individual charges are not independent of each other. This is to be expected from the proximity of the acetate atoms to each other.

It is not possible to visualize the resulting paraboloid in five-dimensional space. However, cross sections of the paraboloid taken at the minimum give a feel for the charge dependence at each atom near the minimum. Figure 8 shows the dependence of $\Delta G_{binding}$ on the charge of each of the four atoms while keeping the charges of the other three atoms at their optimal values. The steeper nature of the O2 curve echoes that observed in the monatomic ligand calculation, although it is even more pronounced here.

The optimal charges obtained were −0.59, −0.13, 0.19, and −0.02 eu for O1, O2, C, and Me, respectively. This pattern of charges qualitatively reproduces what is expected for an acetate molecule. It should be emphasized that we have incorporated in the calculation no information regarding the acetate molecule other that its size, shape, and position in the cathepsin B binding

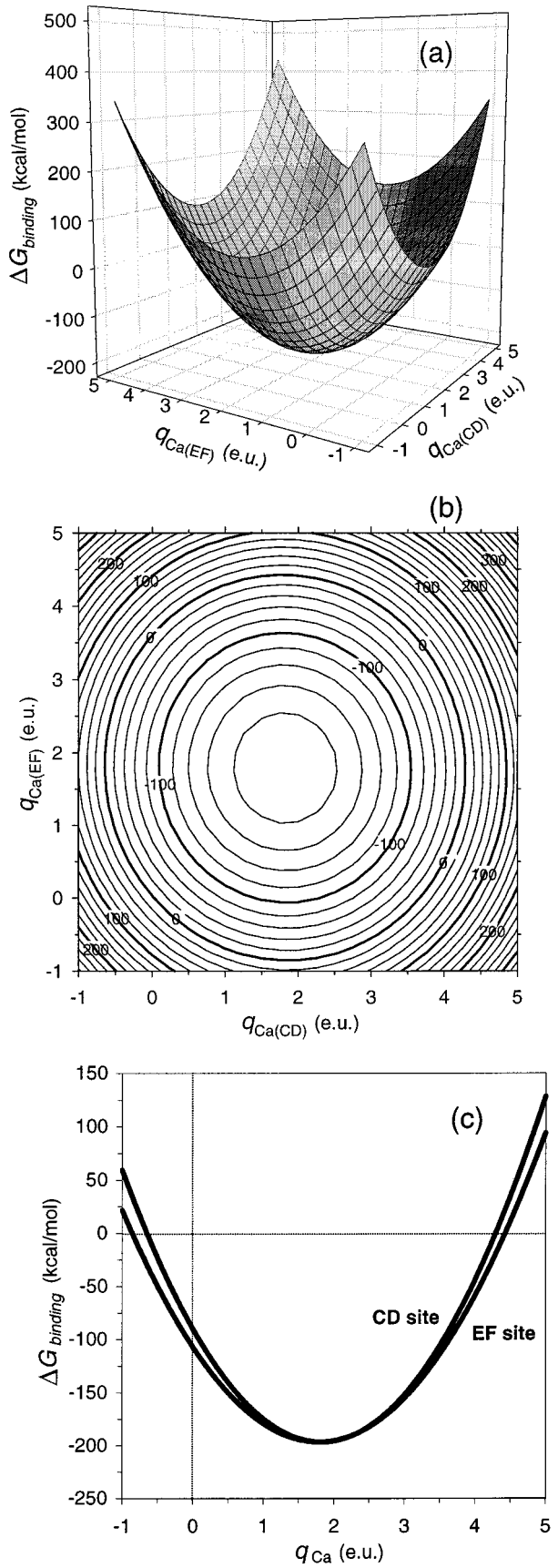

Figure 5. (a) Charge dependence of the binding free energy for the simultaneous binding of calcium ion in the CD and EF calcium-binding sites of parvalbumin. (b) Contour plot of the paraboloid surface in (a). (c) Cross sections of the paraboloid along each of the charge axes.

site. We simply asked what the optimum set of charges such a molecular template should have in order to bind optimally in the S2′ subsite of cathepsin B. The answer returned by the calculation was an acetate-like charge distribution.

The global minimum of the paraboloid corresponds to optimal charges with no constraint on the total charge of the molecule. The resulting net charge of the unconstrained optimal charges is −0.55 eu. If we now impose the constraint that the total charge of the ligand be −1 eu, a new set of charges is obtained (Table 7). We find the new charges to be larger in magnitude than the unconstrained ones: −0.66, −0.57, 0.45, and −0.23 eu for O1, O2, C, and Me, respectively. Table 7 also lists the AMBER partial charges of analogous atoms in the C-terminal proline in CA030. We see that the force field charges are close to our constrained optimal values. This finding suggests that the S2′ subsite of cathepsin B is well-poised to accept the carboxylate moiety of the C-terminal proline group in CA030. For comparison, the last line of Table 7 shows the partial charges of an independent acetate molecule obtained from an ESP-fit at the 6-31G* level. The magnitudes of the charges are somewhat larger, but the similarity to the optimal charges remains.

As mentioned earlier, with four variable charges, the paraboloid for the acetate molecule is a surface in five-dimensional space. However, if we fix the charge of the methyl at its optimum value, then it becomes possible to visualize the dependence of the binding free energy on the other three carboxylate charges by plotting isoenergetic contours (Figure 9). The contours are located in the octant corresponding to negative oxygen and positive carbon charges. We note the anisotropy in the ellipsoidal contours. Also shown in the plot is the proximity of the AMBER and ESP-fit partial charges relative to the optimal values.

Discussion

The receptor molecules used in this study have a range of selectivities for the ligand charge distribution. The 18-crown-6 ether and the parvalbumin calcium-binding sites prefer ligands with highly concentrated charges: +1 or +2 monatomic ions. In contrast, the natural ligand for the cathepsin B active site is a polypeptide with fractional partial charges at the atom centers. It is a measure of the success of the method presented here that the appropriate set of optimized partial charges were identified for each kind of binding site. The calculated optimal charges for the ion-binding sites were between 1 and 2 eu. In cathepsin B, using either monatomic ligands or the multiatomic acetate ligand led to optimized charges of smaller magnitude that were consistent with the typical partial charges found in polypeptide ligands.

In all the calculations described above, we have used a solute dielectric of 2. The choice was motivated as an attempt to take into account solute polarizability, but it is somewhat arbitrary. Dielectric constants in the range of 1−4 are often used in ligand-binding calculations. The choice of dielectric constant will have a significant effect on both the Coulomb and reaction field energies and, consequently, on the calculated binding energies. However, the important question in the context of this work is how the choice of dielectric constant affects the value of the optimum charge. To answer this question, we calculated the dependence on dielectric constant for ligand binding to the 18-crown-6 ether and parvalbumin. Figure 10a shows a plot of the optimum charge versus the dielectric constant. We observe a weak dependence on dielectric constant especially in the range of 1−4. The optimum charges for the ligand are 1.01, 1.02,

TABLE 4: Coefficients for the Dependencies of Various Energy Terms on the Charge of Two Calcium Ions that Bind One to the CD Site and the Other One to the EF Site of Parvalbumin (double site occupancy)

	$c_2(q^2_{Ca(CD)})$	$c_2(q^2_{Ca(EF)})$	$c_1(q_{Ca(CD)}q_{Ca(EF)})$	$c_1(q_{Ca(CD)})$	$c_1(q_{Ca(EF)})$	c_0
E^C_{inter}	–	–	14.0057	−260.4742	−254.2912	–
G^R_{bound}	−15.1171	−19.1519	−13.0326	141.5971	152.1367	−1062.5898
G^R_{Ca}	−47.2703	−47.2703	–	–	–	–
$G^R_{parvalbumin}$	–	–	–	–	–	−1065.5700
$\Delta G^R_{binding}$	32.1532	28.1185	−13.0326	141.5971	152.1367	2.9802
$\Delta G_{binding}$	32.1532	28.1185	0.9731	−118.8771	−102.1545	2.9802

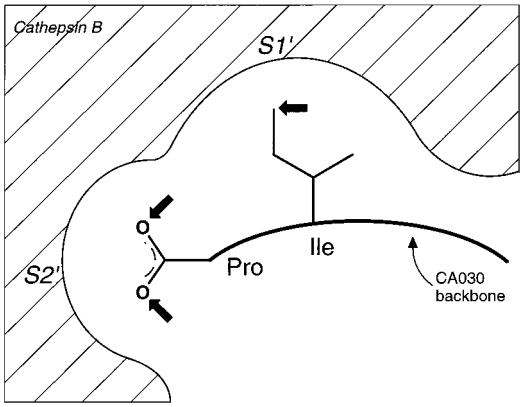

Figure 6. Schematic diagram of the S′ subsites in the active site of cathepsin B. The arrows indicate the positions probed using monatomic ligands.

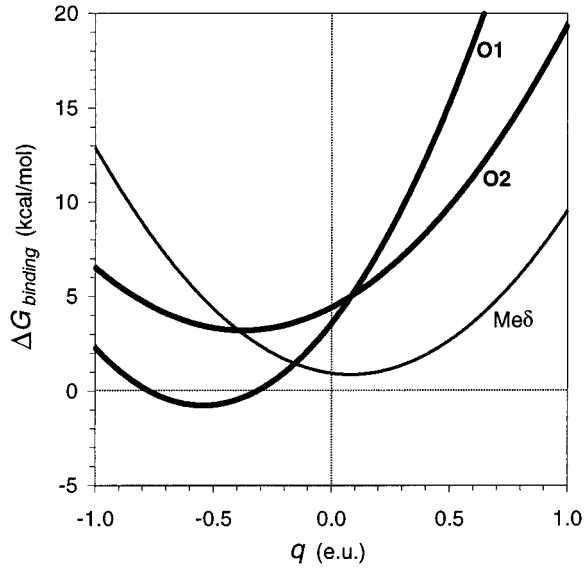

Figure 7. Charge dependence of the binding free energy for each of the monatomic probe positions in the S′ subsites of cathepsin B.

and 1.05 eu for dielectric constants of 1, 2, and 4, respectively. Figure 10b shows the parabolic curves for the charge dependence of the binding energy of a monatomic ligand to 16-crown-6 ether for a series of dielectric constants. We observe that the effect of the dielectric constant is to alter the steepness of the curves but not the location of the minimum. A similar behavior is exhibited by ligand binding to the CD site of parvalbumin. Figure 10a shows a plot of the optimum charge as a function of dielectric constant. The optimum charges are 1.79, 1.85, and 1.97 eu for dielectric constants of 1, 2, and 4, respectively. Figure 10c shows the charge dependence of the binding energy versus dielectric constant. Again, the steepness of the curves is affected but not the location of the minimum. We conclude from this that the choice of dielectric constant is not critical for determining the magnitude of the optimum charge. It is, of course, important for estimating the actual binding energy.

The value of the optimal charge depends on the location of the charge in the binding site and on the ligand cavity shape. An important issue for ligand binding is the sensitivity of the computed optimal charge to the ligand cavity shape. Some indication of the dependence on cavity shape can be gleaned from the cathepsin B example. As described in the Results section, a monatomic ligand has an optimal charge of −0.54 and −0.38 eu at the O1 and O2 locations, respectively. If we recalculate the optimal charge using a ligand cavity defined by the volume enclosed by an acetate molecule but again having a single charge center at either the O1 or O2 site, we obtain optimal charges of −0.53 and −0.50 e.u, respectively, not much changed from the monatomic cavity case.

We also investigated the effect of cavity shape on multiple-charge optimization. Simultaneous optimization of the carboxylate atoms in an acetate ligand cavity yields optimal charges of −0.59, −0.13, and 0.19 eu for the O1, O2, and C atoms, respectively. As an example of a "real-life" situation, we positioned an *N*-acetylproline ligand in the binding mode suggested by the inhibitor CA030 (see the Methods section). We then asked what the optimum charges on the carboxylate of the proline would be in the presence of the volume and charges of the other *N*-acetylproline atoms. The other *N*-acetylproline atoms had partial charges assigned according to the AMBER force field. The calculated optimal charges for the carboxylate atoms were −0.57, −0.10, and 0.20 eu for the O1, O2, and C atoms, respectively. We see that addition of the large proline ring does not alter the value of the optimal charges much. This suggests that the dependence of the optimal charges on cavity shape is fairly local.

The concept of charge optimization has been explored extensively in several recent papers by Tidor and co-workers.[2−6] However, their published work has been limited to the use of spherical cavities to define the dielectric boundaries for the receptor, ligand and complex. In their approach, they calculate the multipole charge distribution that maximizes the binding affinity of a spherical ligand to the receptor. Their method was recently applied to studying ligand binding to barnase, again using spherical cavities for the complex and the ligand.[3] Optimal multipole charge distributions were calculated for a series of spherical ligands with radii ranging from 8 to 11 Å. An atomic charge distribution was then approximated by fitting a set of point charges on a Cartesian grid with 2 Å spacing to best reproduce the multipole charge distribution.[3] The resulting partial charge distribution had plausible magnitudes of <0.7 eu. However, conversion of the charge distribution to an actual molecule was not straightforward.

The use of spherical cavities is a significant limitation since reaction field energies are quite sensitive to the shape and location of the dielectric boundary near the charges of interest. The errors introduced by the spherical cavity approximation make it difficult to apply the method quantitatively to a real

TABLE 5: Coefficients for the Dependencies of Various Energy Terms on the Charge of the Monatomic Ligands that Interact with the Binding Site of Cathepsin B

	O1			O2			Meδ		
	$c_2(q_{O1}^2)$	$c_2(q_{O1})$	c_0	$c_2(q_{O2}^2)$	$c_2(q_{O2})$	c_0	$c_2(q_{Me\delta}^2)$	$c_1(q_{Me\delta})$	c_0
E_{inter}^{C}	–	0.4309	–	–	−16.9671	–	–	−53.1402	–
G_{bound}^{R}	−39.3121	15.4940	−1461.5719	−45.4379	23.3766	−1460.7222	−30.2084	51.4536	−1464.1932
G_{ligand}^{R}	−53.9512	–	–	−53.9512	–	–	−40.4634	–	–
$G_{cathepsihinB}^{R}$	–	–	−1465.1400	–	–	−1465.1400	–	–	−1465.1400
$\Delta G_{binding}^{R}$	14.6391	15.4940	3.5681	8.5133	23.3766	4.4178	10.2550	51.4536	0.9467
$\Delta G_{binding}$	14.6391	15.9249	3.5681	8.5133	6.4095	4.4178	10.2550	−1.6866	0.9467

TABLE 6: Coefficients for the Dependencies of Various Energy Terms on the Atomic Charges of the Acetate Ligand that Binds in the S2′ Subsite of Cathepsin B

	$c_2(q_{O1}^2)$	$c_2(q_{O2}^2)$	$c_2(q_{C}^2)$	$c_2(q_{Me}^2)$	$c_1(q_{O1}q_{O2})$	$c_1(q_{O1}q_{C})$	$c_1(q_{O1}q_{Me})$
E_{inter}^{C}	–	–	–	–	–	–	–
G_{bound}^{R}	−21.9352	−38.9598	−25.7384	−24.2909	−45.8375	−44.2877	−36.5992
$G_{acetate}^{R}$	−47.5820	−47.7512	−37.5770	−38.3938	−61.7142	−73.0685	−55.6600
$G_{cathepsinB}^{R}$	–	–	–	–	–	–	–
$\Delta G_{binding}^{R}$	25.6468	8.7914	11.8386	14.1029	15.8768	28.7808	19.0608
$\Delta G_{binding}$	25.6468	8.7914	11.8386	14.1029	15.8786	28.7808	19.0608

	$c_1(q_{O2}q_{C})$	$c_1(q_{O2}q_{Me})$	$c_1(q_{C}q_{Me})$	$c_1(q_{O1})$	$c_1(q_{O2})$	$c_1(q_{C})$	$c_1(q_{Me})$	c_0
E_{inter}^{C}	–	–	–	0.4309	−16.9671	−14.7068	−29.7569	–
G_{bound}^{R}	−57.2977	−45.6448	−44.9252	26.9258	25.7914	29.7149	39.3093	−1457.2387
$G_{acetate}^{R}$	−73.3599	−55.8622	−63.9373	–	–	–	–	–
$G_{cathepsinB}^{R}$	–	–	–	–	–	–	–	−1465.1400
$\Delta G_{binding}^{R}$	16.0672	10.2173	19.0122	26.9258	25.7914	29.7149	39.3093	7.9013
$\Delta G_{binding}$	16.0672	10.2173	19.0122	27.3567	8.8243	15.0081	9.5524	7.9013

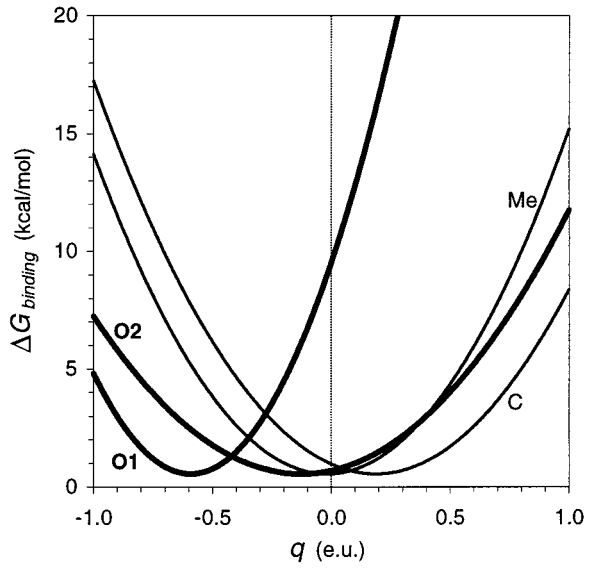

Figure 8. Cross sections along each of the charge axes for the binding free energy paraboloid surface of an acetate ligand in the S′ subsite of cathepsin B.

system. Nevertheless, using charge distributions within spherical cavities, Tidor and co-workers have been able to explore general principles regarding electrostatic contributions to binding affinity and specificity.[5,6] Much like how lattice models in protein folding provide insights on general principles regarding folding, the spherical cavity models studied by Tidor and co-workers provide general insights regarding binding. What we have accomplished in the present paper is to push the concept of charge optimization into the realm of real molecules and irregular dielectric boundaries.

A completely different approach to obtaining optimal charges is the use of free energy derivatives, as exemplified by the work

TABLE 7: Comparison between the Theoretical and Optimal Atomic Partial Charges for the Acetate Ligand that Binds in the S2′ Subsite of Cathepsin B

	O1	O2	C	Me	$\Delta G_{binding}$	$\sum q$
$q_{X\_optimum}$	−0.59	−0.13	0.19	−0.02	0.56	−0.55
$q_{X\_optimum}^{\sum q=-1}$	−0.66	−0.57	0.45	−0.23	2.05	−1.00
$q_{X\_proline}$[a]	−0.77	−0.77	0.66	−0.06	2.19	−0.93
$q_{X\_acetate}$[b]	−0.88	−0.88	1.03	−0.26	2.53	−1.00

[a] AMBER 4.1 partial charges. [b] 6-31G* ESP-fitted partial charges.

of Cieplak et al. on the 18-crown-6 ion system.[31] Their calculations consisted of molecular dynamics simulations with explicit water molecules. As an extension to the method of free energy perturbation, they calculated ensemble averages that are equal to the free energy derivative with respect to the desired variable. One of the derivatives that they looked at was the derivative of the free energy with respect to ion charge. They found the optimal charge for binding to the 18-crown-6 molecule to be close to 1 eu, just as we did. The agreement of our results with those from a full explicit water simulation suggests that the continuum dielectric approximation preserves the essential features of solvation electrostatics.

Conclusion

In this paper, we have shown how we can take the concept of optimal charges beyond model systems and look at real charge distributions with irregular dielectric boundaries. The key to our ability to handle arbitrary molecular shapes and charge distributions is the derivation of a simple analytical expression for the charge dependence of the free energy of binding. Obtaining the coefficients for the expression requires only a few reaction field energy calculations. Given these coefficients, the binding energy can be obtained for any combination of values for the set of charges being studied.

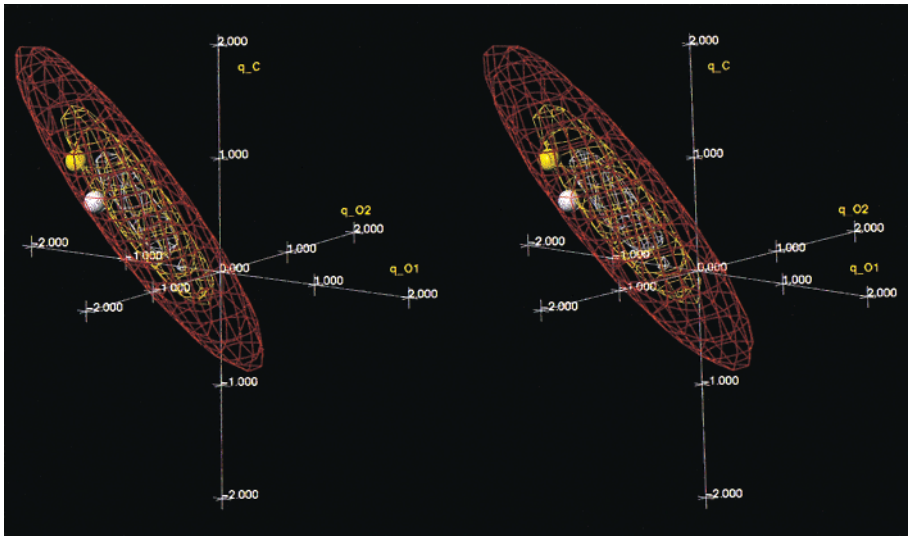

Figure 9. Stereo picture of isoenergetic contours at fixed methyl charge (−0.23 eu; see Table 7) for the acetate ligand in the S′ subsite of cathepsin B. The white sphere marks the AMBER partial charge set corresponding to a proline carboxylate. The yellow sphere indicates the 6-31G* ESP-fit partial charges obtained for an isolated acetate molecule.

This method for determining the optimal charge distribution of a ligand has potential use for molecular design. We can analyze an existing ligand and compare its charge distribution to the optimal one. Differences will suggest atom types that could be changed to lead to the desired charge distribution. Similarly, the effect on the optimal charge distribution of the addition of functional groups can also be calculated. The examples of ligand binding detailed in this paper illustrate how the notion of charge complementarity means not only the pairing of oppositely charged groups but also having the correct magnitude of charge.

Acknowledgment. This is publication number 42966 of the National Research Council of Canada.

Appendix

To derive the charge dependence of the binding free energy on multiple charges, we rewrite eq 10 for the case where multiple charges in m_1 are to be varied

$$G^{\mathrm{R}}_{\mathrm{free}} = \frac{1}{2}\Big[\sum_{k\in K} q_k\Big(\phi^{\mathrm{R}}_k + \sum_{k'\in K-k}\phi^{\mathrm{R}}_{k'} + \phi^{\mathrm{R}}_{m_1-K}\Big) + \sum_{i\in m_1-K} q_i\Big(\sum_{k\in K}\phi^{\mathrm{R}}_k + \phi^{\mathrm{R}}_{m_1-K}\Big) + \sum_{j\in m_2} q_j\phi^{\mathrm{R}}_{m_2}\Big] \quad (19)$$

where K is the set of n charges to be varied. Using eq 13 and regrouping the terms, we can write a multicharge analogue of eq 14

$$G^{R}_{free} = \frac{1}{2}\Big[\underbrace{\sum_{k\in K} q_k^2\phi^{R}_{q_k=1}}_{\text{quadratic}} + \underbrace{\sum_{k\in K} q_k\Big(\sum_{k'\in K-k} q_{k'}\phi^{R}_{q_{k'}=1}\Big)}_{\text{cross-terms}} + \underbrace{\sum_{k\in K} q_k\phi^{R}_{m_1-K} + \sum_{k\in K} q_k\Big(\sum_{i\in m_1-K} q_i\phi^{R}_{q_k=1}\Big)}_{\text{linear}} + \underbrace{\sum_{i\in m_1-K} q_i\phi^{R}_{m_1-K} + \sum_{j\in m_2} q_j\phi^{R}_{m_2}}_{\text{constant}}\Big] \quad (20)$$

Note that in the cross terms, the potential $\phi^{\mathrm{R}}_{q_k'=1}$ (arising from a unit charge at position of charge $q_{k'}$) is evaluated at the position of charge q_k. Similarly, in the linear term, the potential is evaluated at the position of charge q_i. We see that the reaction field energy has a quadratic functional form with respect to the varying charges

$$G^{\mathrm{R}}_{\mathrm{free}} = \sum_{k\in K} c_2(k)q_k^2 + \sum_{k\in K}\sum_{k'\in K-k} c_1(k,k')q_kq_{k'} + \sum_{k\in K} c_1(k)q_k + c_0 \quad (21)$$

The coefficients can be obtained by solving the Poisson equation for a small number of systems. We need n BEM calculations for molecule m_1, in which each varying charge q_k in turn is set to 1 and all other charges are zeroed. Then a BEM calculation is carried out for m_1 with all n varying charges zeroed. Finally, a BEM calculation on m_2 is carried out. Thus, $n + 2$ solutions of the Poisson equation are required to obtain the coefficients for the free state. From eqs 20 and 21, the coefficients are computed as

$$c_2(k) = \frac{1}{2}\phi^{\mathrm{R}}_{q_k=1}(\vec{r}_k)$$

$$c_1(k,k') = \frac{1}{2}\phi^{\mathrm{R}}_{q_{k'}=1}(\vec{r}_k)$$

$$c_1(k) = \frac{1}{2}\Big[\phi^{\mathrm{R}}_{m_1-K}(\vec{r}_k) + \sum_{i\in m_1-K} q_i\phi^{\mathrm{R}}_{q_k=1}(\vec{r}_i)\Big] \quad (22)$$

$$c_0 = \frac{1}{2}\Big[\sum_{i\in m_1-K} q_i\phi^{\mathrm{R}}_{m_1-K}(\vec{r}_i) + \sum_{j\in m_2} q_j\phi^{\mathrm{R}}_{m_2}(\vec{r}_j)\Big]$$

where $\vec{r}_i$ indicates explicitly the position at which the reaction field potential is to be evaluated. (As in eq 13, we note that $\phi^{\mathrm{R}}_{q_k=1}$ has units of potential/unit charge.) To obtain the binding free energy, we perform a similar calculation for the complex, requiring $n + 1$ solutions of the Poisson equation. Thus a total of $2n + 3$ BEM calculations have do be done to obtain the coefficients that will allow the calculation of the binding free energy for any combination of values of the n charges. This is far less than the $2p^n + 1$ calculations that would have to be done in a brute-force grid-scan of the charges with p grid values

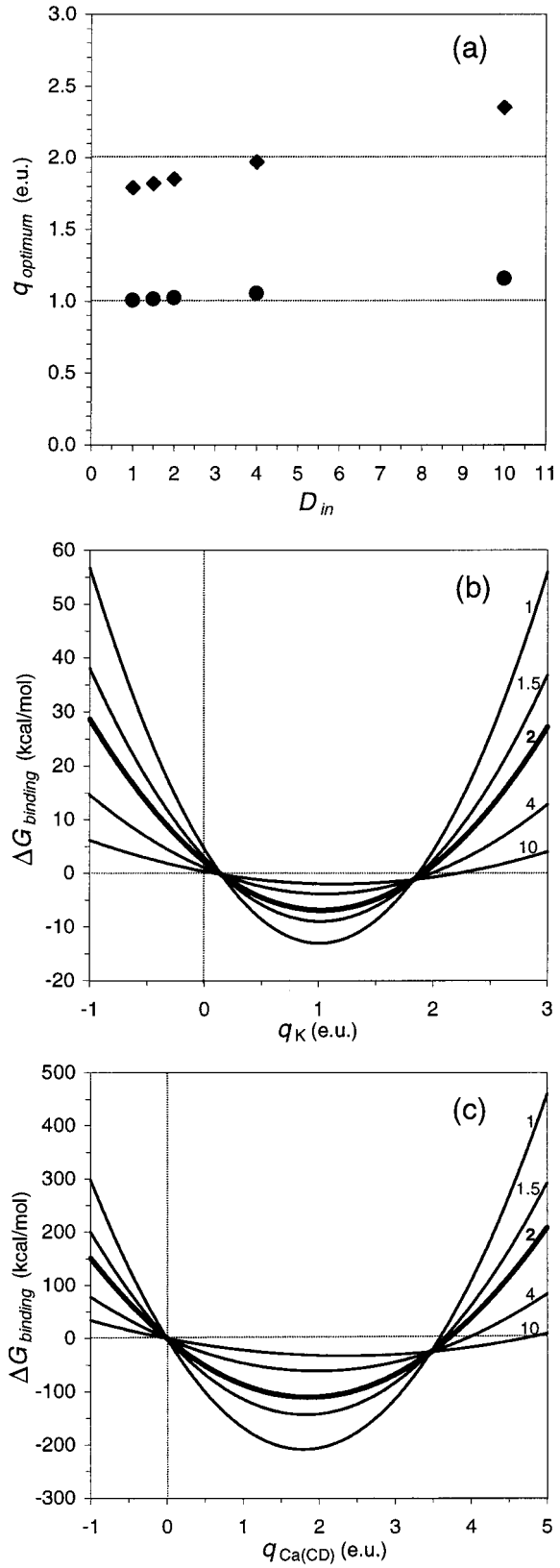

Figure 10. (a) Dependence of the optimal charge on internal dielectric constant. Filled circles represent the binding of a monatomic ligand (K^+ radius) to 18-crown-6 ether. Filled diamonds represent the binding of a monatomic ligand (Ca^{2+} radius) to the CD site of parvalbumin. (b) Charge dependence of the binding energy of a monatomic ligand (K^+ radius) to 18-crown-6 ether. One curve for each of the indicated internal dielectric constants is shown. (c) Charge dependence of the binding energy of a monatomic ligand (Ca^{2+} radius) to the CD site of parvalbumin. One curve for each of the indicated internal dielectric constants is shown.

along each charge axis. For example, for a four-atom ligand such as in our cathepsin B example, a brute-force scan with 10 grid points per charge axis would require 20 001 solutions of the Poisson equation, versus 11 using our analytical method. Also, given the coefficients, finding the minimum of the quadratic form is straightforward and is reduced to solving the system of linear equations obtained by setting the gradient of the quadratic form to zero. The quadratic form implies the existence of a unique minimum. However, depending on the curvature (Hessian) at the minimum, closely related sets of charges may be feasible with little increase in binding free energy cost.

References and Notes

(1) Nicholls, A.; Sharp, K. A.; Honig, B. *Proteins* **1991**, *11*, 281−296.

(2) Lee, L.-P.; Tidor, B. *J. Chem. Phys.* **1997**, *106*, 8681−8690.

(3) Chong, L. T.; Dempster, S. E.; Hendsch, Z. S.; Lee, L.-P.; Tidor, B. *Protein Sci.* **1998**, *7*, 206−210.

(4) Kangas, E.; Tidor, B. *Phys. Rev. E* **1999**, *59*, 5958−5961.

(5) Kangas, E.; Tidor, B. *J. Chem. Phys.* **1998**, *109*, 7522−7545.

(6) Kangas, E.; Tidor, B. *J. Chem. Phys.* **2000**, *112*, 9120−9131.

(7) Zauhar, R. J.; Morgan, R. S. *J. Mol. Biol.* **1985**, *186*, 815−820.

(8) Zauhar, R. J.; Morgan, R. S. *J. Comput. Chem.* **1988**, *9*, 171−187.

(9) Miertus, S.; Scrocco, E.; Tomasi, J. *Chem. Phys.* **1981**, *55*, 117−129.

(10) Tomasi, J.; Persico, M. *Chem. Rev.* **1994**, *94*, 2027−2094.

(11) Cramer, C. J.; Truhlar, D. G. *Chem. Rev.* **1999**, *99*, 2161−2200.

(12) Böttcher, C. J. F. *Theory of Electric Polarization*, 2nd ed.; Elsevier: Amsterdam, 1973.

(13) Byrn, M. P.; Strouse, C. E. *J. Am. Chem. Soc.* **1981**, *103*, 2633.

(14) Howard, A. E.; Singh, U. C.; Billeter, M.; Kollman, P. A. *J. Am. Chem. Soc.* **1988**, *110*, 6984−6991.

(15) Kumar, V. D.; Lee, L.; Edwards, B. F. *Biochemistry* **1990**, *29*, 1404−1412.

(16) Cornell, W. D.; Cieplak, P.; Bayly, C. I.; Gould, I. R.; Merz, K. M., Jr.; Ferguson, D. M.; Spellmeyer, D. C.; Fox, T.; Caldwell, J. W.; Kollman, P. A. *J. Am. Chem. Soc.* **1995**, *117*, 5179−5197.

(17) Turk, D.; Podobnik, M.; Popovic, T.; Katanuma, N.; Bode, W.; Huber, R.; Turk, V. *Biochemistry* **1995**, *34*, 4791−4797.

(18) Hasnain, S.; Hirama, T.; Tam, A.; Mort, J. S. *J. Biol. Chem.* **1992**, *267*, 4713−4721.

(19) Nägler, D. K.; Tam, W.; Storer, A. C.; Krupa, J. C.; Mort, J. S.; Ménard, R. *Biochemistry* **1999**, *38*, 4868−4874.

(20) Purisima, E. O. *J. Comput. Chem.* **1998**, *19*, 1494−1504.

(21) Purisima, E. O.; Nilar, S. H. *J. Comput. Chem.* **1995**, *16*, 681−689.

(22) Vorobjev, Y. N.; Hermans, J. *Biophys. J.* **1997**, *73*, 722−731.

(23) Purisima, E. O.; Sulea, T.; Vasilyev, V. *J. Phys. Chem. B*, submitted for publication.

(24) Åqvist, J. *J. Phys. Chem.* **1990**, *94*, 8021−8024.

(25) Rashin, A. A.; Namboodiri, K. *J. Phys. Chem.* **1987**, *91*, 6003−6012.

(26) Rashin, A. A.; Honig, B. *J. Phys. Chem.* **1985**, *89*, 5588−5593.

(27) Burgess, M. A. *Metal Ions in Solution*; Ellis Horwood: Chichester, England, 1978.

(28) Marcus, Y. *Ion Solvation*; John Wiley: New York, 1985.

(29) Izatt, R. M.; Terry, R. E.; Haymore, B. L.; Hansen, L. D.; Dalley, N. K.; Avondet, A. G.; Christensen, J. J. *J. Am. Chem. Soc.* **1976**, *98*, 7620−7626.

(30) van Eerden, J.; Harkema, S.; Feil, D. *J. Phys. Chem.* **1988**, *92*, 5076−5079.

(31) Cieplak, P.; Pearlman, D. A.; Kollman, P. A. *J. Chem. Phys.* **1994**, *101*, 627−633.